

Chapter 2

Activity Driven Phase Separation and Ordering Kinetics Of Passive Particles

Abbreviations/Acronyms: **ABP** (active Brownian particle), **ABPs** (active Brownian particles), **CSD** (cluster size distribution), **HCP** (Hexagonal close-packed structure), **MIPS** (motility induced phase separation), **PDF** (probability distribution function), **PSOP** (phase separation order parameter), **RDF** (radial distribution function).

2.1 Introduction

In the recent studies, it is found that collection of active Brownian particles (ABPs) undergoes a motility induced phase separation (MIPS) without any cohesion at packing density much lower than the density for phase separation in corresponding passive systems (Bechinger et al., 2016; Dolai et al., 2018; Marchetti et al., 2013; Ramaswamy, 2010; Romanczuk et al., 2012b). Unlike for other active particle systems, where alignment interaction among the particle is responsible for the phase separation Bechinger (2016); Chaté et al. (2008b); Singh & Mishra (2020); Vicsek et al. (1995), the mechanism of phase separation in ABPs is due to the enhanced persistent motion of active particles (Alaimo &

[Voigt, 2018](#); [Cates & Tailleur, 2015b](#)).

Recent researches have focused the kinetics and steady state of pure ABPs or in the mixture of passive particles ([Angelani et al., 2011](#); [Di Leonardo et al., 2010](#); [Kümmel et al., 2015](#); [Ray et al., 2014](#); [Singh & Mishra, 2020](#)). In a recent work of [Stenhammar et al. \(2015\)](#), a monodisperse mixture of active passive particles is studied for varying activity and packing fraction of ABPs. Whereas in other studies a field theoretic approach is used to understand the propagation of active passive interface in the mixture of passive and active particles [Wysocki et al. \(2016\)](#). In the study of [Wittkowski et al. \(2017\)](#), a mixture of active passive particle is studied, and different phases and dynamics of system is studied. A variety of interesting properties and phases have been found when ABPs are placed in the mixture with passive particles. Asymmetric passive particles lead to directional transport and trapping when placed in the sea of ABPs [Buttinoni et al. \(2013b\)](#); [Malgaretti & Stark \(2017\)](#); [Pattanayak et al. \(2019b\)](#); [Reichhardt & Reichhardt \(2018\)](#). Having the property of the directed motion, these systems can be used for effective drug delivery. Mixture of active and passive particles lead to phase separation and segregation phenomena [Dolai et al. \(2018\)](#). This property is useful for particle sorting and separation in industrial processes. These properties of such systems make them useful in industrial and pharmaceutical applications. Symmetric passive particles in the mixture of ABPs has also been used as a probe to characterise the properties of ABPs [Beatrice et al. \(2017\)](#); [Patteson et al. \(2016\)](#); [Wu & Libchaber \(2000\)](#). Experiments on the dynamics of large passive beads in active bacterial fluid show the persistence motion of bead in bacterial solution [Wu & Libchaber \(2000\)](#). In the binary mixture of ABPs with passive bead, large passive particles experience an effective attractive interaction analogous to depletion induced attraction in asymmetric equilibrium binary mixture [Dolai et al. \(2018\)](#); [Liu et al. \(2020\)](#); [Patteson et al. \(2016\)](#).

Most of the above studies of binary active-passive mixture are studied where passive

particles are bigger in size and treated as a probe to characterise the properties of active medium [Kümmel et al. \(2015\)](#); [Ni et al. \(2013, 2014\)](#) or monodisperse mixture of active passive particles and dynamics of different phases are explored [Stenhammar et al. \(2015\)](#); [Wittkowski et al. \(2017\)](#); [Wysocki et al. \(2016\)](#). This chapter is about addressing the question that how the ABPs which are bigger in size can influence the characteristics of athermal passive particles ? The system resembles big microorganisms moving in passive fluid. In general thermal and hydrodynamic effects are important in normal passive fluid, but we ignore it here to make the model simple and only study the effect of activity on the properties of passive particles.

We consider a minimal model of mixture of small passive and big active Brownian particles on a two-dimensional substrate. The both types of particles interact through a short range soft repulsive interaction. The dynamics of active particles is driven by the active self-propulsion force and interaction with the particles in its surroundings whereas passive particles can move only due to the interaction with other particles. The packing fraction of both particles are same and total packing fraction is kept fixed at 0.6. The dynamics and steady state of passive particles are studied for various size ratios of active and passive particles and dimensionless activity of ABPs.

Our main results are as follows: Starting from the random homogeneous mixture of active and passive particles, passive particles start to phase separate with time. The phase separation order parameter of passive particles grows with time and reaches a steady state with ~ 1 for large size ratio and activity and remains much lower than 1 for small size ratio and activity. Hence a phase diagram is found in the plane of size ratio and activity. For moderate size ratio and activity the clustered passive particles form hexagonal close packed structures and start to overlap for large size ratio and activity. The cluster size distribution changes from exponential to power law and power converges to -2 . Hence passive particles form the spanning clusters [Rapaport \(1992\)](#) for larger size ratio and

activity.

We further studied the kinetics of the phase separation. The mass of the largest cluster grows as a power law with time, with a much slower growth kinetics in contrast to conserved passive equilibrium and active systems [Ahmad et al. \(2010\)](#); [Ni et al. \(2013\)](#); [Pattanayak et al. \(2021a,b\)](#)

Rest of the chapter is divided in the following manner. In next section [2.2](#), we describe the model in detail. Section [2.3](#) discusses the results of our study and finally in section [2.6](#) we conclude our results.

2.2 Model

We consider a binary mixture of small athermal passive particles in the presence of large active Brownian particles (ABPs) on a two-dimensional substrate. The active and passive particles are modeled as discs of radius r_a and r_p respectively. We choose $r_a > r_p$, active particles are larger in size compare to passive particles. The size ratio $S = \frac{r_a}{r_p}$ is one of the control parameters in the model. The radius of the passive particles is kept fixed and radius of active particles is tuned to vary the size ratio. We keep the packing fractions of both types of particles $\phi_a = \frac{\pi r_a^2 N_a}{L^2} = \phi_p = \frac{\pi r_p^2 N_p}{L^2} = 0.3$, hence the number of active particle N_a are less in comparison to that of passive particles N_p . Both active and passive particles are defined by their position $\mathbf{r}_i(t)$ and active particles are also having their orientation $\theta_i(t)$, which determines their direction of self-propulsion. They self-propel along their direction of orientation $\theta_i(t)$ with a constant self-propulsion speed v_0 . The dynamical Langevin's equations of motion for position and orientation of active particles are

$$\frac{d\mathbf{r}_i^a(t)}{dt} = v_0 \hat{\mathbf{n}}_i(t) + \mu \mathbf{F}_i(t) \quad (2.1)$$

where $\mathbf{n}_i(t) = (\cos(\theta_i(t)), \sin(\theta_i(t)))$ is the unit direction of self-propulsion of ABP.

The change in the orientation of the active particle is given by:

$$\frac{d\theta_i}{dt} = \sqrt{v_r} \eta_i(t) \quad (2.2)$$

here $\eta_i(t)$ is the random Gaussian white noise with mean zero and variance, $\langle \eta_i^r(t) \eta_j^r(t') \rangle = \delta_{ij} \delta(t - t')$, where v_r is the rotational diffusion constant of active particles. The equation of motion for the passive particle is given as:

$$\frac{d\mathbf{r}_i^p(t)}{dt} = \mu \mathbf{F}_i(t) \quad (2.3)$$

Here, the mobility, μ is chosen to be the same for both types of particles. $\mathbf{F}_i(t)$ is the force acting on the i^{th} particles, due to all other particles interacting with it

$$\mathbf{F}_i(t) = \sum_{j \neq i} \mathbf{F}_{ij}(t) \quad (2.4)$$

The force is obtained from the soft-repulsive pair potential $\mathbf{F}_{ij} = -\nabla U(r_{ij})$, where $U(r_{ij}) = K(r_{ij} - (r_{\alpha i} + r_{\alpha' j}))^2$ if $r_{ij} \leq (r_{\alpha i} + r_{\alpha' j})$ and 0 otherwise. $r_{ij} = |r_i - r_j|$ and K is the force constant and r_α , is the radius of active or passive particles for α and $\alpha' = a$ or p respectively. v_r^{-1} is the time scale over which the orientation of an active particle changes. Hence, $l_p = v_0 v_r^{-1}$, is the persistence length or run length, is the typical distance travelled by an active particle before it changes its direction. In our study, $l_p = (100r_p \text{ to } 600r_p)$ is tuned by tuning SPPs v_0 . The $(\mu K)^{-1} = 0.7$ defines the elastic time scale in the system. We define the dimensionless activity $\bar{v} = \frac{l_p}{r_p}$ as the ratio of persistent length to the size of passive

particles. The size ratio S and \bar{v} are the two tuning parameters in the model. A schematic cartoon of system is shown in Fig. 2.1, where red big particles are ABPs and small gray particles are passive. The white dots on red particles represent their instantaneous direction of orientation θ .

We start with random non-overlapping arrangement of active and passive particles on a two dimensional square substrate of linear dimension $L = 250r_p$ with periodic boundary condition. The equations 2.1 – 2.3, are updated and one simulation step is counted after updation of all the particles once. The time step $\tau = 5 \times 10^{-4}$ and total 6×10^4 simulation steps are used to get the results. We have used 20 independent realisations to get averaged data and different realisations are obtained by initialising the system with the similar initial conditions but different configurations. We first characterise the effect of size ratio and activity on the steady state of the athermal passive particles in the mixture. Then we study the kinetics to the steady state.

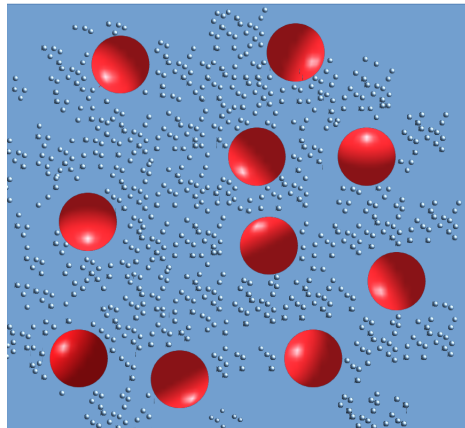


Fig. 2.1 (color online) Schematic diagram of the model. It shows the initial homogeneous state of the system. Here the colours and sizes represent two types of particles. Bigger particles (red) are active particles and smaller particles (grey) are passive particles. Small white dot on red particles denote the instantaneous orientation direction θ of ABPs.

2.3 Results

We start with the random homogeneous distribution of active and passive particles and the equations 2.1 – 2.3 are integrated to update the position and orientation of active and position of passive particles. In Fig. 2.2 we plot the time evaluation snapshot of local density of passive particles at different times = 0.05, 0.5 and 30.0 and for two different size ratios $S = 10$ and 6 and for $\bar{v} = 100, 300$ and 600. The bright and dark regions show the lower and higher local density of passive particles respectively. Local density ρ_p is defined as: *the number of passive particles in the small coarse-grained area* ($a = 5r_p \times 5r_p$). In Fig. 2.2(h-i) we plot the probability distribution function (PDF) of local density $P(\rho_p)$ for the same parameters as in Fig. 2.2(a-f). The tail of the distribution is larger for large size ratio $S = 10$ and activity $\bar{v} = 600$. As time progresses the passive particle starts to come close to each other. Hence local density ρ_p of passive particle rich region grows or passive particles phase separate. To characterise the phase separation, we calculate the phase separation order parameter (*PSOP*), $\phi(t)$. The analogy of (*PSOP*) comes from standard liquid gas phase separation Pathria (2016). Using the same analogy, in our system we define (*PSOP*), as $\phi(t) = \langle (n_p(t) - n_a(t)) / (n_p(t) + n_a(t)) \rangle$, where $n_p(t)$ and $n_a(t)$ are calculated as the number of active and passive neighboring particles around a passive particle. $\langle .. \rangle$ means average over all passive particles and 20 independent realisations. With the above definition if passive particles are mainly surrounded by passive particles then the $\phi(t)$ will be close to 1 and if, found in the mixture of active and passive, then it will be close to 0. With time $\phi(t)$ grows and approaches a steady state. We calculate the steady state $\phi = \langle \phi(t) \rangle_t$, where $\langle .. \rangle_t$ is the average of $\phi(t)$ over a time interval in the steady state. In Fig. 2.2(g) we plot the phase diagram in the plane of activity and size ratio (S, \bar{v}). The color shows the magnitude of *PSOP*, $\phi(t)$. For large activity and size ratio, phase separation increases in the system.

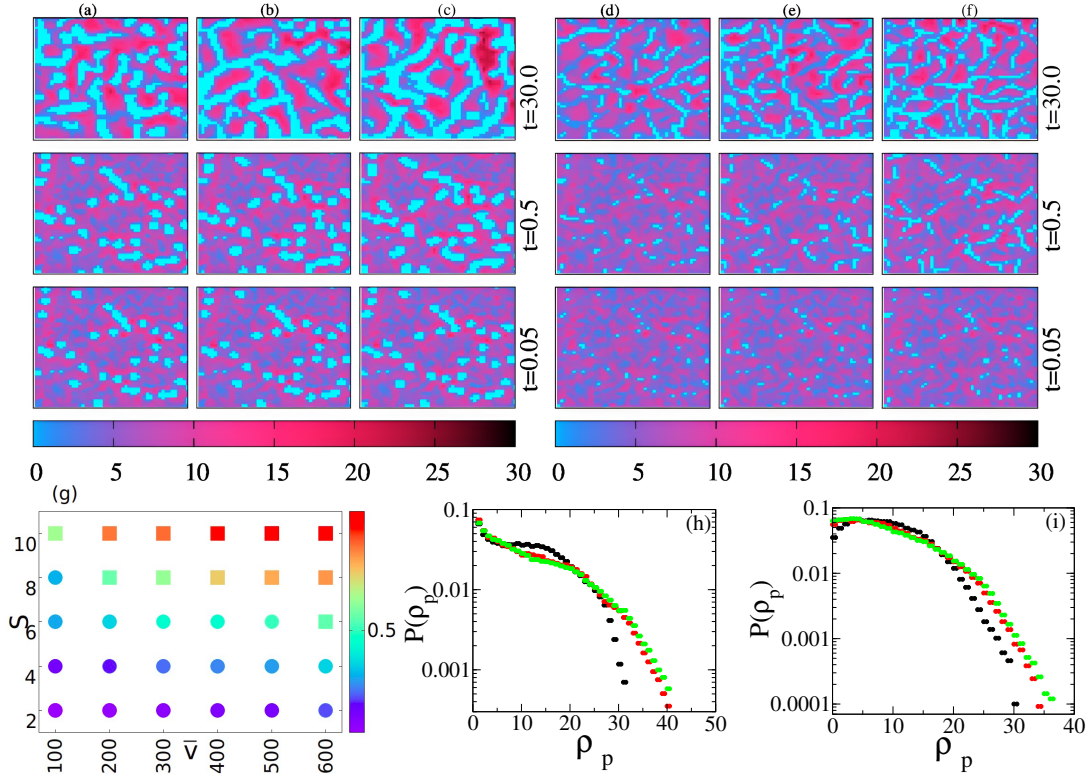


Fig. 2.2 (color online) The real space snapshots of local density of passive particles at different times. (a-c) are for size ratio 10 and $\bar{v} = 100, 300$ and 600 respectively. (d-f) are for size ratio 6 and $\bar{v} = 100, 300$ and 600 respectively. From bottom to top panels are for times, $t = 0.05$, $t = 0.5$ and $t = 30.0$. The color bar shows the local density of passive particles. (g) The lower color plot shows the phase separation order parameter ($PSOP$) in the plane of size ratio and activity (S, \bar{v}). (h-i) Probability distribution function (PDF) of local density of passive particles $P(\rho_p)$ is plotted for two different size ratios 10 and 6 ((h) and (i)) respectively and for three $\bar{v} = 100, 300$ and 600 .

2.4 Characteristics of steady state

2.4.1 Radial distribution function (RDF) $g_{pp}(r)$

As discussed in previous section, system shows the phase separation for larger size ratio and activity. Hence clustering increases with increasing S and \bar{v} . We further characterise the structure of the clusters by calculating the radial distribution function (RDF) of passive-passive particles for different size ratio S and \bar{v} . The RDF , $g_{pp}(r)$ gives the probability of finding a passive particle at a radial distance r from the center of the given passive particle.

In Figure 2.3 we plot the $g_{pp}(r)$ vs. scaled distance r/r_p , for passive-passive particles for three different activities $\bar{v} = 100, 300$ and 600 and varying the size ratio $S = 6, 8$ and 10 . For small activity and $S = 6$ as shown in Fig. 2.3(a), the first peak appears at $r/r_p \approx 2$ and second peak is at 4 and few more higher order peaks are present. But as we increase $S > 8$, the location of first peak remains almost the same but a small hump in second peak appears at $r/r_p = 2\sqrt{3}$, which is due to the presence of hexagonal close packed structure (HCP) in the clusters. Also for $S > 6$, higher order peaks are more pronounced. The zoom in plot in Fig. 2.3(a) (inset) shows the enlarged second peak for three $S = 6, 8$ and 10 . As we increase, $\bar{v} = 300$, the location of the first peak shifts at distance smaller than $r/r_p \approx 2$, which suggests overlapping particles due to soft repulsive interaction. The second peak of $g_{pp}(r)$ appears at $r/r_p \approx 2\sqrt{3}$, for size ratio $S > 6$, hence HCP structure of clusters. Also the distinct higher order peaks are found for larger size ratio $S > 8$. Again the inset Fig.2.3(b) shows the zoom in second peak of the $g_{pp}(r)$. On further increasing $\bar{v} = 600$, the first and second peak of $g_{pp}(r)$, systematically shifts towards the small scaled distance, hence more overlapping particle clusters, the distinct nature of higher order peaks decreases on increasing S . As we increase S and activity, the passive particles start to overlap and it leads to weaker periodic clusters as shown in the inset Fig. 2.3(c). The figure shows the zoom in second peak, where the structure in second peak has been disappeared for large activity $\bar{v} = 600$. In the bottom panel of Fig. 2.3(d-f) we show the zoom in structure of particle clusters for $\bar{v} = 300$ for size ratios $S = 6, 8$ and 10 respectively. As it is very clear that for this intermediate activity $\bar{v} = 300$ (Fig. 2.3(b)) as we increase S the periodicity within the cluster increases.

Hence using *RDF*, we find the periodic *HCP* nature of particle clusters first increases on increasing activity and size ratio and again for very large $\bar{v} = 600$ and $S = 10$, overlapping large clusters. Now we further characterise the characteristics of large clusters by calculating the cluster size distribution (*CSD*) of different size clusters.

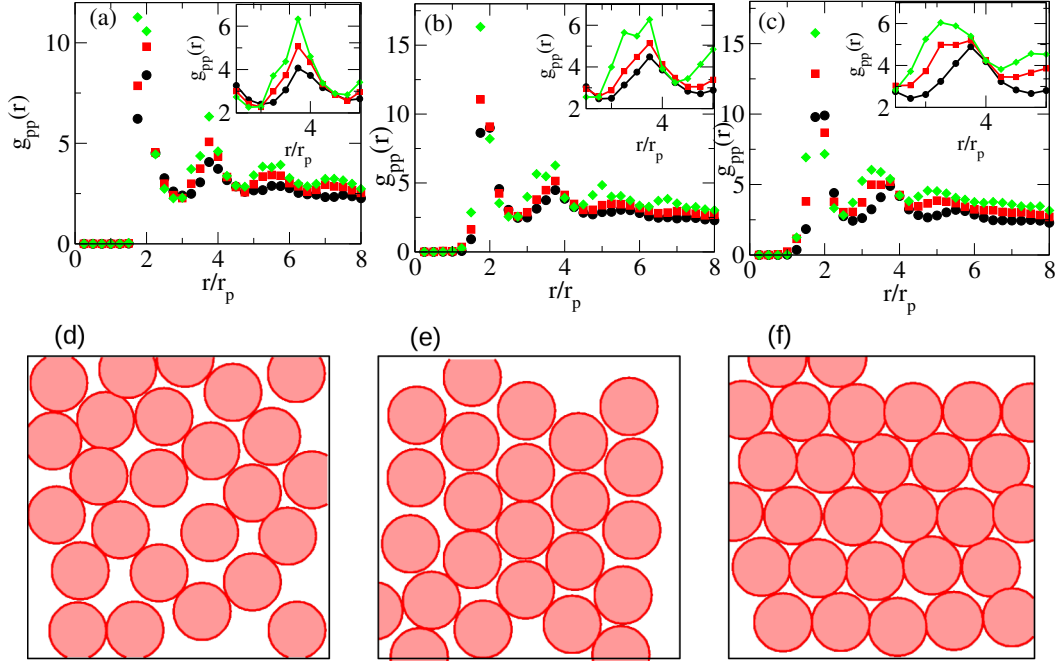


Fig. 2.3 (color online) Passive-passive radial distribution function (RDF), $g_{pp}(r)$ is plotted for different parameters. (a-c) is for fixed activity and varying size ratio. \bar{v} is varied for three different values, 100, 300 and 600. (a) is for $\bar{v} = 100$ (b) is for $\bar{v} = 300$ and (c) is for $\bar{v} = 600$ and size ratio S is taken 6, 8 and 10 for black \circ , red \square and green \diamond respectively. inset figures are zoomed for the same parameters as mentioned in (a), (b) and (c). At the bottom (d), (e) and (f) are real space (zoomed) snapshots to support the cluster formation by fixing the activity $\bar{v} = 300$ and $t = 30$ for size ratios 6, 8 and 10 respectively.

2.4.2 Cluster size distribution (CSD)

To further understand the characteristics of clusters we calculate the probability distribution function of different sized clusters. A cluster is defined as set of particles connected by a distance smaller or equal to $2r_p$ (*diameter of the particle*). A cluster of size n has n —*particles connected cluster*. Then we calculate the number of different sized cluster in the total system. In this manner, all particles are part of a single particle cluster. Hence number of clusters of size $n = 1$ is total number of particles [Dolai et al. \(2018\)](#). We further calculate the fraction of cluster of size n , or cluster size distribution (CSD). In Fig. 2.4 we plot the normalised cluster size distribution (CSD) $P(n)/P(1)$, where $P(i)$ is obtained from the counting all the clusters of size $i = 1, 2, \dots, n$. In Fig. 2.4(a) we plot the CSD for

activity $\bar{v} = 100$ for three different size ratios $S = 6, 8$ and 10 . For small activity, $\bar{v} < 300$ and size ratio $S < 8$, the *CSD* decay exponentially at $n > 20$. Hence for small activity and size ratio we find small clusters and particles are well separated from each other (as shown in Fig. 2.4(b)). Hence weak clusters as found in the *RDF*, $g_{pp}(r)$ plot as shown in Fig. 2.3(a). As we increase size ratio $S > 6$, for $\bar{v} = 100$, clustering increases and *CSD* decay as a power law. The power approaches -2.5 for large size ratio $S = 10$. The real space snapshots of particles show the enhanced clustering on increasing S . For moderate activity $\bar{v} = 300$, *CSD* for small size ratio $S = 6$, is exponential with large exponential tail and for large size ratio $S > 6$, the exponential tail approaches to power law tail -2 . Also the real space snapshots show the clustering increases on increasing S . But for larger size ratio $S = 10$, particles start to overlap and HCP structure weakens as shown in Fig. 2.3(b). As we further increase activity $\bar{v} = 600$, the *CSD* is power law for all size ratios $S = 6, 8$ and 10 and power slowly converges to -2 for largest size ratio 10 . The power -2 suggest that for large activity passive particles form the percolating clusters spanning the whole system ?.

2.5 Growth kinetics

After understanding the steady state properties of the mixture, we study the kinetics of phase separation of athermal passive particles. We study the kinetics of growing cluster by calculating the mass of the largest cluster at different times, $\langle m(t) \rangle$. In Figure 2.5, we plot the $\langle m(t) \rangle$ for two different size ratios $S = 10$ and 6 and for different \bar{v} . where $\langle .. \rangle$ is mean over 50 independent realisations. In Fig. 2.5(a) we plot $\langle m(t) \rangle$ for size ratio 10 for three different activities $\bar{v} = 100, 300$ and 600 . For all activities and $S = 10$, at very early time $t < 10^{-2}$, $\langle m(t) \rangle$ grows with time and then for an intermediate times $t (10^{-2}, 10)$, growth becomes slow and $\langle m(t) \rangle$ develops a plateau and again starts to

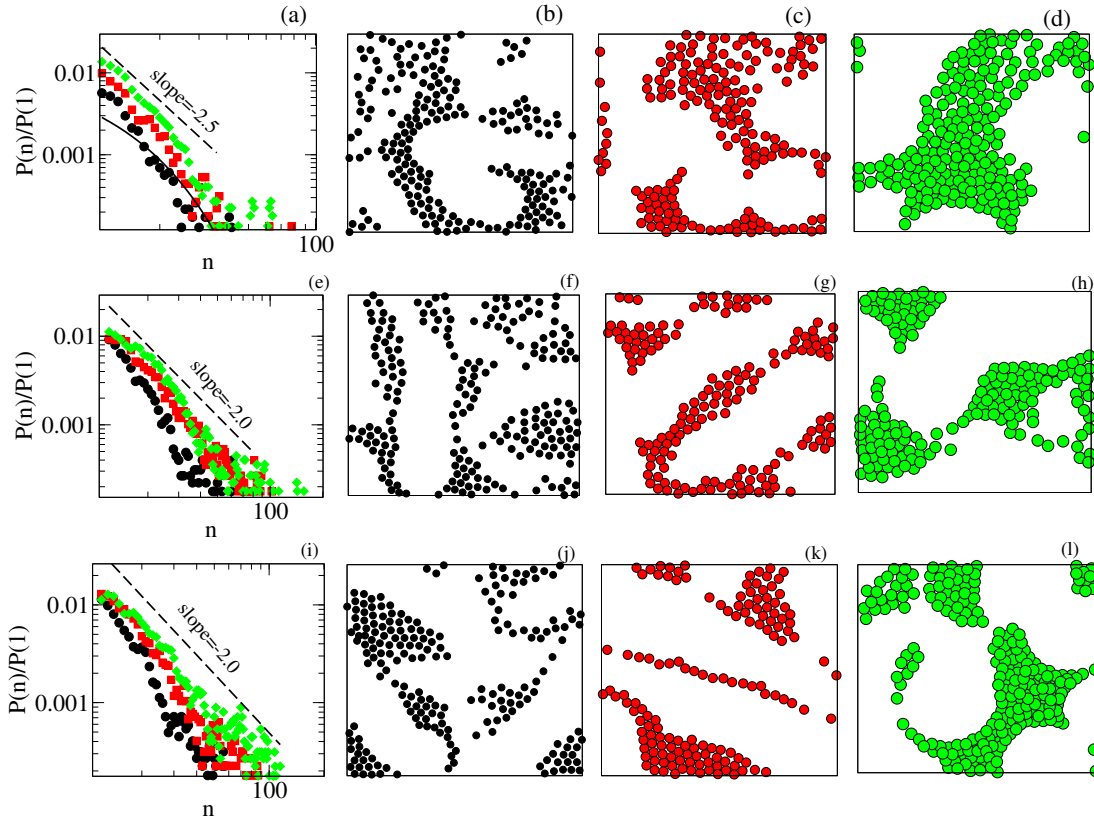


Fig. 2.4 (color online) Cluster size distribution (*CSD*) and real space snapshots of part of the system are plotted for different parameters. Different panels (a-d) are for fixed $\bar{v} = 100$, (e-h) are for $\bar{v} = 300$ and (i-l) are for $\bar{v} = 600$ and black, red and green colors are for size ratios 6, 8 and 10 respectively. *CSD* is shown in (a), (e) and (i) for $\bar{v} = 100, 300$ and 600 respectively and for size ratio 6, 8 and 10. Symbols have the same meaning as in Fig. 2.3.

grow for late times $t \geq 10$. The plateau region decreases with increasing activity. Since activity is enhancing the clustering in passive particles. The only mechanism of motion of passive particles are due to the interaction of them with other passive and active particles. For small activity and size ratio, active particles have lesser probability to interact with passive particles, hence slower dynamics of passive particles. This lead to stucking of them for some intermediate times. At late times, they do experience the effect of active particles and show the enhance motion and hence clustering. This is the reason for the decrease in the plateau region for larger activity and size ratio. For $S = 6$ and small $\bar{v} = 100$, the very early time ($t \simeq 0.001 - 0.02$), when the initial configuration equilibrate, dynamics

is fast and hence the $\langle m(t) \rangle$ grows with time. Then particles are stuck in regions with not many active particles in their surroundings hence slow dynamics and we experience a plateau region for intermediate time ($t \simeq 0.02 - 10$) Fig. 2.5(c-d). Then they further get more interaction with active particles and $\langle m(t) \rangle$ grow as $t^{1/3}$ with time for late time ($t \simeq 10 - 100$) Fig. 2.5(e-f). After time $t \simeq 90$ the $\langle m(t) \rangle$ shows saturation due to finite system size. Increasing the activity leads the passive particles to spend less time in the intermediate time region and so the size of the plateau decreases with increasing activity. The late time growth of $\langle m(t) \rangle \sim t^{1/3}$ for all activities. In Fig. 2.5(right panel) we show the plot of $\langle m(t) \rangle$ for size ratio $S = 6$. The growth of $\langle m(t) \rangle$ shows the same behaviour as for $S = 10$ Fig. 2.5(right panel), only the plateau region is increased for $S = 6$. For the largest activity \bar{v} and size ratio $S = 10$, $\langle m(t) \rangle$ increases monotonically with time t with $\langle m(t) \rangle \sim t^{1/3}$.

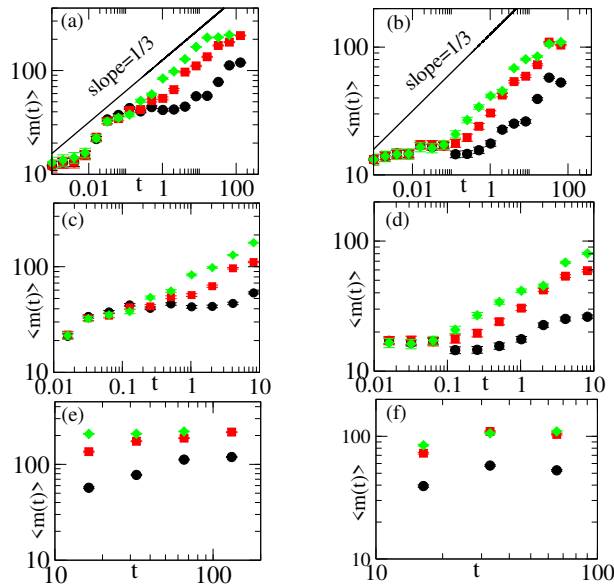


Fig. 2.5 (color online) Mean mass of the largest cluster $\langle m(t) \rangle$ is plotted for activities $\bar{v} = 100, 300$ and 600 . Left panel is for size ratio 10 and right panel is for size ratio 6. Black circles (\bullet); red squares (\blacksquare); green diamonds (\blacklozenge) show the activities 100, 300 and 600 respectively. Straight line is the line with slope 1/3. (c), (d) and (e), (f) are the zoomed plot for intermediate ($t \simeq 0.01 - 10$) and late time ($t \simeq 10 - 100$) region for the same parameters.

2.6 Conclusion

We have studied the phase separation and ordering kinetics of a binary mixture of passive and active Brownian particles on a two-dimensional substrate with periodic boundary condition. The passive particles are smaller in size comparison to the ABPs. The ABP moves along the direction of their heading and both types of particles interact through a short range soft core repulsive interaction. Hence the dynamics of passive particles are only due to interaction force among the particles. The system is studied for various size ratios S and activities \bar{v} of active particles. We focus our study on the steady state and kinetics of small passive particles in the presence of big passive particles. Starting from the random homogeneous state, the clustering of small passive particle is measured by calculating phase separation order parameter (*PSOP*). The *PSOP* is small for size ratio $S < 6$ and small activity $\bar{v} < 300$, whereas for large size ratio $S > 8$ and higher activity $\bar{v} > 300$, *PSOP* approaches ~ 1 . The clusters of passive particles are random small clusters for small size ratio and activity and HCP structures are formed for intermediate size ratio $S = 8$ and activity $\bar{v} = 300$ and then overlapping clusters are found for large size ratio and activity $S > 8$ and $\bar{v} = 300$. The Cluster size distribution decays exponentially for small size ratio and activity and approaches to a power law decay with exponent -2 for large size ratio and activity. The power law decay with power -2 indicates the formation of connected clusters as in [Rapaport \(1992\)](#) for large size ratios and activities.

We have also calculated the kinetics of growing cluster of passive particles. The mean mass of the largest cluster grows with time as a power law. The growth law is much smaller than the conserved growth kinetics of corresponding equilibrium and active Brownian systems [Bray \(1994\)](#); [Pattanayak et al. \(2021a,b\)](#); [R. Wittkowski & Cates \(2014\)](#); [Stenhammar et al. \(2013\)](#).

Hence our study gives the steady state of collection of passive particles moving under the effect of dynamics of active Brownian particle. It focuses on the steady state and kinetics

for binary mixture where passive particles are much smaller than the ABPs. The system resembles the effect of big microorganism moving in passive medium.
